Strong shifts in diabatic nondynamic electron correlations cause conical intersection between lowlying closedshell adiabatic singlets of like symmetry in ozone

Gregory J. Atchity and Klaus Ruedenberg

Citation: The Journal of Chemical Physics **99**, 3790 (1993); doi: 10.1063/1.466229
View online: http://dx.doi.org/10.1063/1.466229
View Table of Contents: http://scitation.aip.org/content/aip/journal/jcp/99/5?ver=pdfcov
Published by the AIP Publishing

Strong shifts in diabatic nondynamic electron correlations cause conical intersection between low-lying closed-shell adiabatic singlets of like symmetry in ozone

Gregory J. Atchity and Klaus Ruedenberg
Ames Laboratory, U.S. Department of Energy and Department of Chemistry, Iowa State University, Ames, Iowa 50011

(Received 15 March 1993; accepted 19 May 1993)

Using the quantum chemical construction of diabatic states from adiabatic states formulated in the subsequent paper, the lowest two $^1A_1$ states of ozone are expressed in terms of its diabatic components and the interaction matrix H_{ij} between them is determined. An analysis of the electronic structure of the diabatic states leads to an understanding of the reasons for the sign changes in ΔH and H_{12} and, hence, for the conical intersection between these two low-lying closed-shell adiabatic states of like symmetry.

I. INTRODUCTION

The two lowest $^1A_1$ potential energy surfaces of ozone, which we have mapped out in C_{2v} symmetry in a previous investigation,[1] are notable for several reasons. First, the ground state surface has *two minima*—the experimentally observed open structure, with an angle of 116°, and the, as yet, experimentally unobserved equilateral triangle ring structure. The ring minimum lies about 30 kcal/mol above the open minimum and slightly above the dissociated species O_2+O. Second, less than 0.04 Å away from the *transition state* between the ring and open structures of the ground state, the *second* $^1A_1$ state has a *minimum*. Finally, these two states of like symmetry were found to *cross in a conical intersection* within 0.04 Å of the aforementioned upper state minimum and the ground state transition state. Since this seems to be the first instance of an intersection between the two lowest closed-shell states of like symmetry in the vicinity of their minima in a common molecule, it is of interest to learn the causes for such a crossing. In the present investigation, we look for the *electronic structure features* which are related to the discovered intersection.

The existence of the two minima is a consequence of the fact that there exist two closed-shell electronic structures, A and B say, with different stabilities in different parts of the internal coordinate space. For the equilateral minimum, structure A is more stable than structure B, whereas for the open minimum, structure B is more stable than structure A. If both structures are of the closed-shell singlet type, as is the case here, then one typically encounters an *avoided crossing* near the transition state. In the case at hand, the two states become, however, degenerate at the crossing point.

In the language of the fundamental analysis of surface crossings,[2] the two electronic structures A and B correspond to two *diabatic* states ϕ_1 and ϕ_2 from which the two adiabatic states ψ_1 and ψ_2 can be constructed. The change in stability between ϕ_1 and ϕ_2 implies that, near the ridge of the potential energy surface, which separates the catchment basins of the two minima in the C_{2v} restricted two-dimensional coordinate space, the energy difference

$$\Delta H = H_{11} - H_{22} = \langle \phi_1 | H | \phi_1 \rangle - \langle \phi_2 | H | \phi_2 \rangle \qquad (1)$$

changes sign. Along this ridge, the two adiabatic states are closest in energy. A true intersection will occur if, somewhere along the line $\Delta H = 0$, the additional condition

$$H_{12} = \langle \psi_1 | H | \psi_2 \rangle = 0 \qquad (2)$$

is also satisfied. In general, it can be expected that the off-diagonal element H_{12} will also change sign in this case and the degeneracy of the two states occurs where the curves $H_{12}=0$ and $\Delta H=0$ intersect.

If the diabatic states (and, hence, the adiabatic states) belong to *different* irreducible representations, then the reason for the vanishing of H_{12} is trivially obvious and the explanation of the intersection reduces to a rationalization of the sign change of ΔH, i.e., of the change in the relative stabilities of the diabatic states. If, on the other hand, the diabatic states (and, hence, the adiabatic states) are *of like symmetry*, then the explanation of the intersection also requires an answer to the additional, more complex question of why H_{12} changes sign.

If both diabatic states are represented by closed-shell single determinants differing in one doubly occupied orbital only, then H_{12} is an exchange integral between the two differing orbitals and always positive so that an intersection is precluded. This inference remains presumably valid when each of the two diabatic states is dominated throughout by a single determinant, i.e., when both contain *dynamic* electron correlations only, and it must be for this reason that intersections between closed-shell singlets of like symmetry have not previously been encountered. The $1\,^1A'$ and $2\,^1A'$ states of ozone furnish a first example of two such states which, in fact, do cross. An understanding of the factors that lead to their intersection may thus be of value for the prediction of similar crossings in other systems.

It stands to reason that such an understanding is likely to be gained from an examination of the energetics of the *diabatic* states. Accordingly, an electronic structure analysis in terms of diabatic states is undertaken in the present investigation. The adiabatic $1\,^1A_1$ and $2\,^1A_1$ states are decomposed in terms of two diabatic states, which are determined by the method formulated in the subsequent paper,[3] and the critical quantities ΔH and H_{12} are calculated over the entire region of interest in coordinate space. The elec-

 0021-9606/93/99(5)/3790/8/$6.00

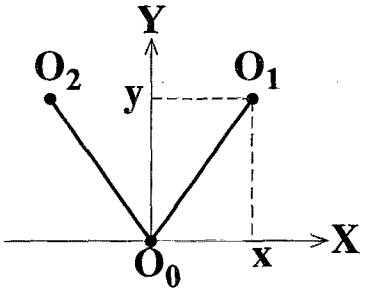

FIG. 1. Internal coordinates for ozone in C_{2v}.

tronic structure analysis of the diabatic states then leads to an appreciation of the reasons for the sign changes of ΔH and H_{12} which entail the conical intersection. From what has been said above, one would surmise that the diabatic states embody strong *nondynamic* electron correlations and this is in fact found to be the case.

We are not aware of previous investigations of this type of problem.

II. THE ADIABATIC AND DIABATIC POTENTIAL ENERGY SURFACES

A. Coordinate space

We choose the coordinates x and y defined through Fig. 1 as the two internal coordinates for the C_{2v} restricted deformations of ozone. The center atom is at the origin and the two end atoms are at mirror image positions with respect to the y axis.

The potential energy surfaces were calculated at the approximately 500 points shown as dots in Fig. 2. Special

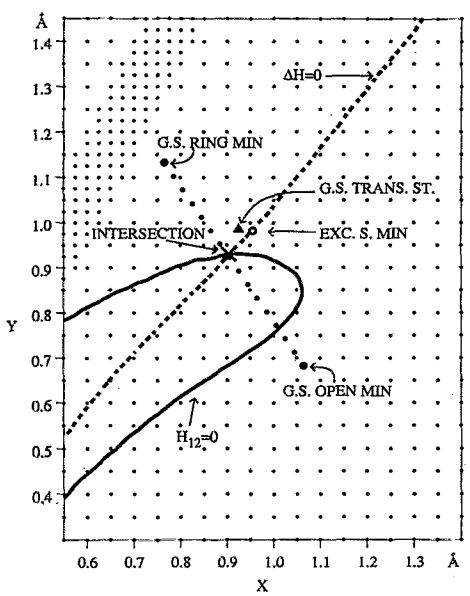

FIG. 2. Data points calculated in C_{2v}. Dots mark the points at which energies are calculated. Medium size dots: the path between lower surface minima. Large dots: lower surface minima. Empty dots: upper surface minima. Triangles: ring-opening transition state. ×: intersection between the surfaces. Solid line: $H_{12}=0$. Dashed line: $\Delta H=0$.

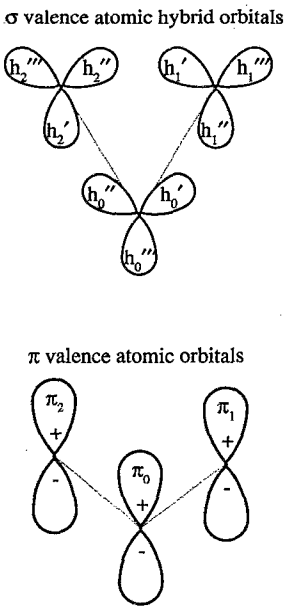

FIG. 3. A schematic drawing of the active valence orbitals of ozone.

symbols in the figure mark the various critical points of the two surfaces. A particular sequence of dots marks the line from one ground state minimum to the other through the intersection point. Also shown are the curves $\Delta H=0$ and $H_{12}=0$, which will be determined in the sequel (dashed line and solid line).

B. Orbital space

The full valence space is the configuration space spanned by all configurations that can be formed from the set of 12 orbitals which can be perceived as molecule-deformed minimal basis atomic orbitals ("quasiatomic orbitals") on the three oxygens.[4] They are depicted schematically in Fig. 3. Nine of them are symmetric with respect to the molecular plane ("σ type," A' irrep in C_s symmetry). From them one obtains the bonding-adapted σ molecular orbitals

$$\begin{aligned} h_{01} &\approx N_+(h_0'+h_1''), \quad h_{01}^* \approx N_-(h_0'-h_1''), \\ h_{12} &\approx N_+(h_1'+h_2''), \quad h_{12}^* \approx N_-(h_1'-h_2''), \\ h_{02} &\approx N_+(h_2'+h_0''), \quad h_{02}^* \approx N_-(h_2'-h_0''). \end{aligned} \tag{3}$$

The remaining three quasiatomic orbitals are antisymmetric with respect to the molecular plane ("π type," A'' irrep in C_s).

Appropriate linear combinations of the quasiatomic orbitals belong to irreps of $C_{2v}(A'\to A_1,B_2;\ A''\to A_2,B_1)$. For the σ orbitals, one has in particular

$$h_{12}=\sigma_+ : A_1, \quad h_{12}^*=\sigma_- : B_2. \tag{4}$$

The symmetry and bonding adapted π-type orbitals are of the form

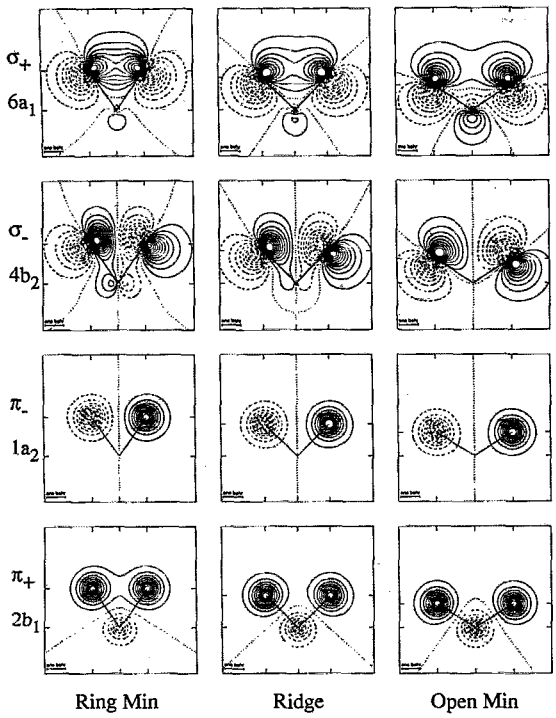

FIG. 4. The molecular orbitals of ozone at the three critical points on the path between the two ground state minima. Solid lines: positive contours. Dashed lines: negative contours. Dotted lines: zero contours. The σ orbitals are plotted in the plane of the molecule. The π orbitals are plotted in a plane slightly above the plane of the molecule.

$$\begin{aligned} &\pi = c_0\pi_0 + c_+(\pi_1+\pi_2): && B_1, \\ &\pi_- = c_-(\pi_1-\pi_2): && A_2, \\ &\pi_+ = c_0'\pi_0 - c_+'(\pi_1+\pi_2): && B_1. \end{aligned} \tag{5}$$

Figure 4 displays contour plots of the natural orbitals resulting from the actual multiconfiguration self-consistent field (MCSCF) calculations which correspond to the discussed orbitals σ_+, σ_-, π_+, and π_- for three points on the line leading from one minimum to the other (see Fig. 2). The character of these orbitals manifestly changes very little and they remain clearly identifiable along the entire path.

C. Configuration space

Using the C_{2v} adapted orbitals, the full valence space consists of 4067 configurations. MCSCF optimizations in this space yield the FORS[4] wave functions of our previous investigation.[1] An examination of these wave functions reveals that, in the entire region around the intersection and the open minimum (i) the orbitals h_{01}^* and h_{02}^* have very small occupations and (ii) all other orbitals are doubly occupied, except the orbitals σ_+, σ_-, π_+, and π_- whose occupations vary in the region of interest. This distribution of occupation numbers arises from the fact that, in this region, the wave function is *dominated* by the four valence configurations

$$\begin{aligned} |14,4,+\rangle &= |\sigma^{14}\pi^4+\rangle = |(\sigma^{10}\pi^2)\sigma_+^2\sigma_-^2\pi_+^2\rangle, \\ |14,4,-\rangle &= |\sigma^{14}\pi^4-\rangle = |(\sigma^{10}\pi^2)\sigma_+^2\sigma_-^2\pi_-^2\rangle, \\ |12,6,+\rangle &= |\sigma^{12}\pi^6+\rangle = |(\sigma^{10}\pi^2)\pi_+^2\pi_-^2\sigma_+^2\rangle, \\ |12,6,-\rangle &= |\sigma^{12}\pi^6-\rangle = |(\sigma^{10}\pi^2)\pi_+^2\pi_-^2\sigma_-^2\rangle \end{aligned} \tag{6}$$

where

$$\sigma^{10} = (h_0''')^2(h_1''')^2(h_2''')^2(h_{01})^2(h_{02})^2. \tag{7}$$

It is obvious that for the ring minimum, where the symmetry is D_{3h}, additional configurations will have comparable weight, namely those obtained by the following substitutions:

$$\begin{aligned} &\text{(i)}\ \ \sigma_- = h_{12}^* \rightarrow h_{01}^* \text{ or } h_{02}^*, \quad \textit{in } |14,4,+\rangle \textit{ and } |14,4,\rangle \\ &\text{(ii)}\ \ h_{01} \rightarrow h_{01}^* \text{ or } h_{02} \rightarrow h_{02}^*, \quad \textit{in } |12,6,+\rangle. \end{aligned} \tag{8}$$

Since our objective is the elucidation of the intersection, we choose as the dominant configurations of the adiabatic states only the four listed in Eq. (6). The dominance of these configurations in ψ_1 and ψ_2 is shown in Table I. In each of the four cases, the first listed configuration is the one with the lower energy, which survives in the SCF approximation, whereas the configuration listed second provides correlation to the first.

We anticipated that the implementation of the methodology proposed in the subsequent paper[3] had to be elaborated in detail and required considerable testing as we went along and, hence, that wave functions would have to be evaluated at many points. We therefore decided to begin by carrying through the procedure in a configuration space of a dimension less than 4067. In fact, we limited the configuration space to the four configurations given in Eq. (6). It should be noted that the determination of the matrix T which yields the diabatic states *would proceed no differently* than in the present calculations and the numerical values obtained for T_{ij} would be very little, if at all different if the calculations were based on the corresponding four dominant configurations of the *full* FORS wave function. The main difference would be that, in the end, the transformation T would be applied to the adiabatic states ψ_1 and ψ_2 expanded in terms of the 4067 FORS configurations. Preliminary calculations of this kind have, in fact, yielded results in close agreement with those reported here.[5]

D. Potential energy surfaces

1. Adiabatic states

The adiabatic states $1\,^1A_1$ and $2\,^1A_1$ were determined by two-state-averaged MCSCF calculations in the space of the four configurations of Eq. (6). The orbitals were ex-

TABLE I. Dominant configurations in the $1\,^1A_1$ and the $2\,^1A_1$ states.

	Open basin		Ring basin	
Ground state $1\,^1A_1$	$\|\sigma^{14}\pi^4-\rangle$,	$\|\sigma^{14}\pi^4+\rangle$	$\|\sigma^{12}\pi^6+\rangle$,	$\|\sigma^{12}\pi^6-\rangle$
Excited state $2\,^1A_1$	$\|\sigma^{12}\pi^6+\rangle$,	$\|\sigma^{12}\pi^6-\rangle$	$\|\sigma^{14}\pi^4-\rangle$,	$\|\sigma^{14}\pi^4+\rangle$

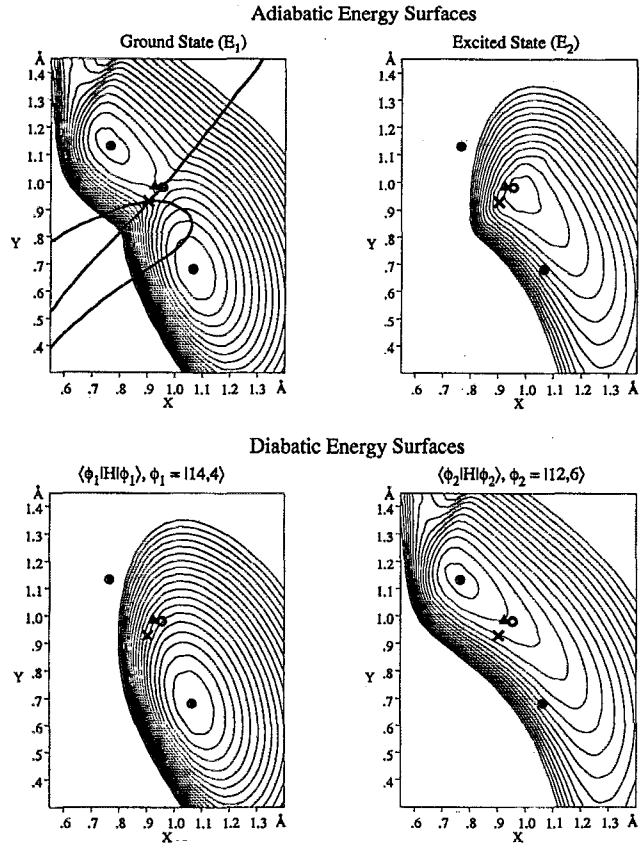

FIG. 5. Energy surfaces of the lowest two $^1A_1$ states of ozone in C_{2v}. Solid dots: minima of the lower surface. Empty dots: minimum of the upper surface. Triangle: ring-opening transition state. ×: the intersection between the surfaces. Solid lines mark $H_{12}=0$ and $\Delta H=0$. Contour increment: 10 mhartree.

panded in terms of a Dunning–Hay ($9s5p1d/3s2p1d$) basis of 45 segmented contracted atomic orbitals.[6] (The d orbitals were of the Cartesian type with $\zeta_d=0.85$.) The calculations were performed with the program MOLPRO of Werner and Knowles.[7]

Contours of the two surfaces are displayed in the upper two panels of Fig. 5. These surfaces qualitatively reproduce all features of the FORS (i.e., 4067 configuration) potential energy surfaces with one exception—the ring minimum does not have D_{3h} symmetry. This is, of course, due the fact that we have omitted the correlating configurations required by D_{3h} symmetry mentioned in the preceding section. Table II compares the critical points of the two surfaces obtained by the present wave function with those of the FORS wave function. The good qualitative agreement is a consequence of the dominance of the four configurations in the FORS wave function.

2. Diabatic states

From the adiabatic states, we determined the diabatic states by the procedure described in the subsequent paper.[3] From the dominance Table I, it is apparent that one of the diabatic states must be dominated by the two $(\sigma^{14}\pi^4)$ configurations throughout, whereas the other diabatic state

TABLE II. A comparison of geometries of critical points determined with four configuration MCSCF wave functions to those determined with FORS wave functions.

	Four configuration MCSCF		FORS (4067 configurations)	
	θ	R	θ	R
Open minimum	114.69	1.265	116.32	1.298
Ring minimum	68.10	1.366	60.00	1.470
Upper minimum	88.43	1.370	83.59	1.441
Transition state	86.40	1.351	83.86	1.431
Intersection	88.38	1.375	83.18	1.476

must be dominated by the two $(\sigma^{12}\pi^6)$ configurations everywhere. Accordingly, we call the diabatic states

$$\phi_1=|\sigma^{14}\pi^4\rangle=|14,4\rangle, \quad \phi_2=|\sigma^{12}\pi^6\rangle=|12,6\rangle, \qquad (9)$$

respectively, *even though both are linear combinations of all four configurations.* Consequently, in Eq. (10) of the subsequent paper, the index α was taken to cover the two $(\sigma^{14}\pi^4)$ configurations and the index β taken to cover the two $(\sigma^{12}\pi^6)$ configurations. The quantities R_{ij} were evaluated, $\cos\beta$ and $\sin\beta$ were calculated, and the elements of the transformation matrix **T** were determined at each point shown in Fig. 2. In Sec. V of the subsequent paper, we have discussed the precautions that must be taken in order to guarantee continuity of the diabatic states.

Contours of the surfaces of the diabatic states are displayed in the lower panels of Fig. 5. It is apparent that each of the two diabatic states has a minimum which coincides with one of the two minima of the adiabatic ground state. In agreement with Table I, it is apparent that the diabatic state $\phi_1=|14,4\rangle$ is more stable than $\phi_2=|12,6\rangle$ near the open structure, whereas the state $\phi_2=|12,6\rangle$ is more stable than $\phi_1=|14,4\rangle$ near the ring structure.

On all four panels of Fig. 5, all critical points are marked. (On the first one, the lines $\Delta H=0$ and $H_{12}=0$ to be discussed below are also shown.)

III. QUANTITATIVE ANALYSIS OF THE INTERSECTION

A. The surfaces of ΔE, $\Delta H(x,y)$, and $H_{12}(x,y)$

The difference ΔE between the two adiabatic state energies is displayed in Fig. 6. In agreement with Fig. 5, ψ_1 is the ground state and ψ_2 is the excited state. The difference is seen to be very small all along the ridge separating the basins of the two ground state minima which, as we shall see below, is in fact the line given by $\Delta H=0$. The graph at lower right, plotting ΔE along this line, shows the typical pattern of the conical intersection at the point marked by a cross on the enlarged panel at the lower left.

The crucial quantities for the elucidation of the intersection are the functions $\Delta H(x,y)$ and $H_{12}(x,y)$ obtained from the diabatic states according to Eqs. (1) and (2). As a first step in our analysis, we examine the contour maps of ΔH and H_{12} in order to establish where they change sign. The contours are displayed on the two panels on the left hand side of Fig. 7, where negative values are indicated by

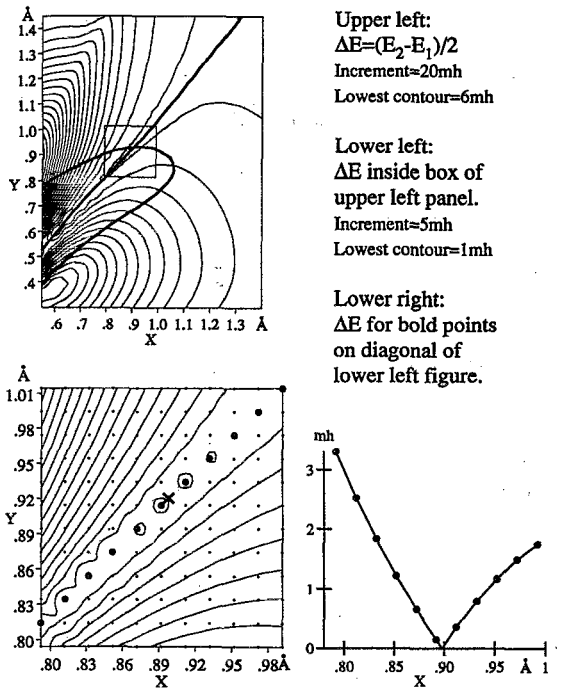

FIG. 6. The energy difference $\Delta E=(E_2-E_1)/2$.

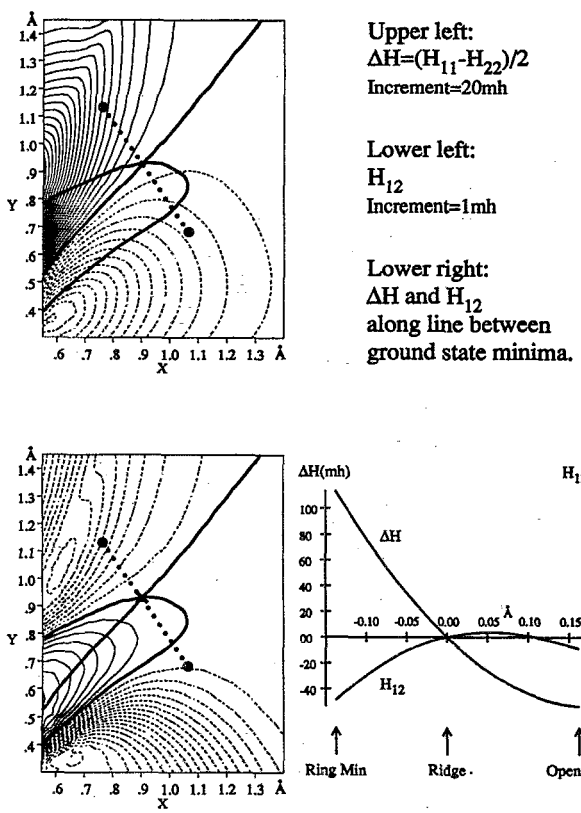

FIG. 7. The surfaces of ΔH and H_{12}. Large dots: minima of the lower surface. Small dots: the path between the minima. Solid lines: $\Delta H=0$ and $H_{12}=0$. Negative contours are dashed. Positive contours are solid. Zero contours are bold and solid.

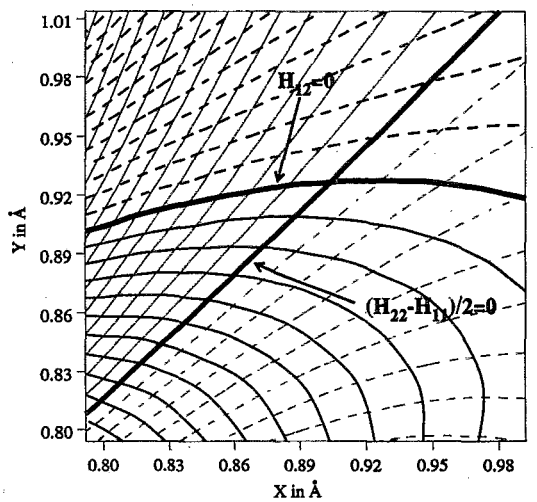

FIG. 8. Contours of ΔH and H_{12} near the intersection. Solid lines: positive contours. Dashed lines: negative contours. Bold solid lines: zero contours. The lines $\Delta H=$const (running approximately diagonal from lower left to upper right) and $H_{12}=$const (running approximately horizontal) can be inferred from the lines $\Delta H=0$ and $H_{12}=0$. Contour increments: $\Delta H=5$ mhartree; $H_{12}=0.168$ mhartree.

broken lines, positive values by solid lines, and zero contours by bold-faced solid lines. Both contours $\Delta H=0$ and $H_{12}=0$ are shown on both panels in order to identify the intersection. They were also shown on Fig. 2 and on the upper left panels of Figs. 5 and 6 so as to show that this intersection coincides indeed with the surface crossing, as required by theory. The upper left panel of Fig. 5 shows that the line $\Delta H=0$ is a straight line following the ridge separating the ring minimum basin from the open minimum basin of the ground state. Figure 6 shows that the two adiabatic surfaces are very close along this entire line.

Figure 8 displays the region around the intersection in greater detail. A comparison with Fig. 6 suggests that an accurate determination of the intersection point may be more efficiently accomplished through the intersection of $\Delta H=0$ and $H_{12}=0$ than by finding the point where ΔE vanishes.

The graph at the lower right of Fig. 7 displays a quantitative plot of ΔH and H_{12} along the dotted line which connects the two minima and passes through the intersection (see Fig. 2).

In the subsequent sections, we shall address the question of how the variation of ΔH and H_{12} along the line connecting the two minima, as displayed by Fig. 7, can be related to the electronic structures of the diabatic states. As a first step towards the answer, we examine the wave functions of these states.

B. Wave functions

1. Diabatic states

We begin by examining the configurational expansions of the two diabatic states

$$\phi_1=|\sigma^{14}\pi^4\rangle=|14,4\rangle, \quad \phi_2=|\sigma^{12}\pi^6\rangle=|12,6\rangle. \qquad (9)$$

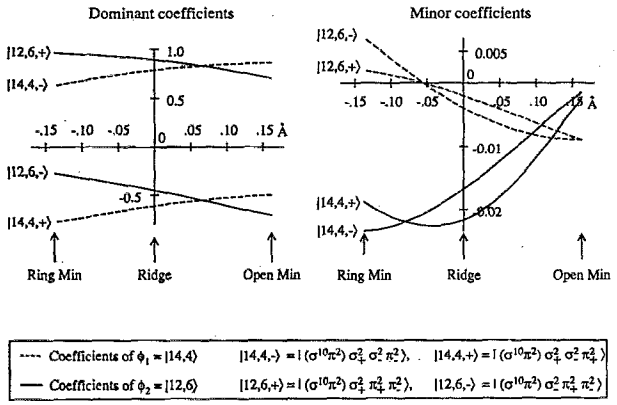

FIG. 9. Variation of the coefficients of the diabatic states along the path between the ground state minima.

As mentioned above, both of them are linear combinations of all four configurations, but we expect that $|14,4,+\rangle$ and $|14,4,-\rangle$ dominate in $|14,4\rangle$ and that $|12,6,+\rangle$ and $|12,6,-\rangle$ dominate in $|12,6\rangle$. This is indeed borne out by Fig. 9 which exhibits plots of the four coefficients of the two states along the line connecting the minima. *Note the difference in the ordinate scale* between the dominant and the minor coefficients.

Essential for the question to be discussed here is, however, the following additional observation:

within each diabatic state, the relative weight of the two dominant configurations changes significantly.

Examination of the left hand side of Fig. 9 reveals the pattern formulated in Table III. The coefficient relationships implied by this table can be understood as follows:

near the ring minimum, the configurations $|14,4,+\rangle$ and $|14,4,-\rangle$ have approximately equal weight because the molecular orbitals (MOs) π_+ and π would be degenerate for D_{3h} symmetry. However, near the open minimum, π is a nonbonding orbital, whereas π_+ is an antibonding orbital so that $|14,4,-\rangle$ is more stable than $|14,4,+\rangle$. On the other hand, the configurations $|12,6,+\rangle$ and $|12,6,-\rangle$ have approximately equal weight for the open structure since here the MOs σ_+ and σ_- are almost degenerate because, due to the distance between the end atoms, the bonding–antibonding effect is small. For the ring structure, however, the two end atoms have come close together so that σ_+ is a bonding MO and σ_- is an antibonding MO. Hence, $|12,6,+\rangle$ is more stable than $|12,6,-\rangle$.

TABLE III. Relative weights of the two dominant configurations in the diabatic states $|14,4\rangle$ and $|12,6\rangle$.

Configurations in diabatic states	Ring minimum	Open minimum
$\|14,14,+\rangle$ in $\|14,4\rangle$	Approximately	Small
$\|14,4,-\rangle$ in $\|14,4\rangle$	equal weights	Large
$\|12,6,+\rangle$ in $\|12,6\rangle$	Large	Approximately
$\|12,6,-\rangle$ in $\|12,6\rangle$	Small	equal weights

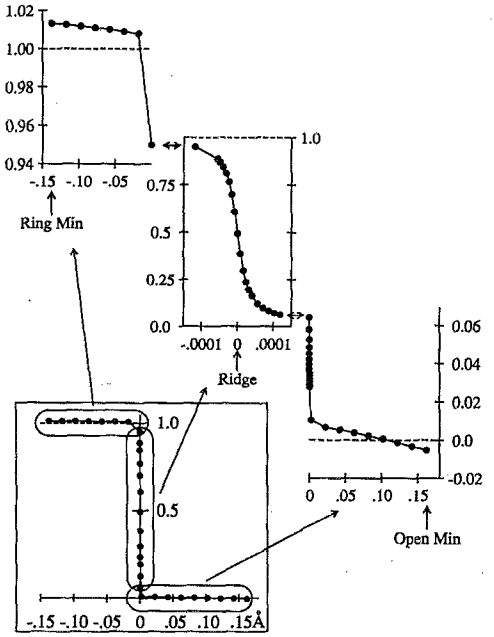

FIG. 10. Angle of rotation from diabatic to adiabatic states along the path between the ground state minima. Abscissa=distance from the ridge in Ångstroms. Ordinate=the angle in units of $\pi/2$.

2. Superposition of diabatic states

The adiabatic states are expressed in terms of the diabatic states by a transformation matrix **T** which is given by a rotation angle γ as follows:

$$\psi_1 = \phi_1 \cos\gamma - \phi_2 \sin\gamma, \quad \psi_2 = \phi_1 \sin\gamma + \phi_2 \cos\gamma, \qquad (10)$$

in agreement with Eqs. (1) and (3) of the subsequent paper. The calculated variation of this angle along the line connecting the two minima is shown in Fig. 10. The graph at the lower left displays the overall variation of $\gamma/(\pi/2)$. The other graphs display enlarged presentations for three different regions. The plots exhibit the change in dominance of the two diabatic states in the two adiabatic states upon crossing the ridge between the two ground state basins. For the open minimum, $\gamma \approx 0$, so that $\psi_1 \approx \phi_1 = |14,4\rangle$ = the ground state and $\psi_2 \approx \phi_2 = |12,2\rangle$ = the excited state, whereas, for the ring minimum, $\gamma \approx \pi/2$ so that the converse holds. The plots also show that the change near the ridge is extremely sudden. The changeover would be discontinuous if the line connecting the minima would pass *exactly* through the intersection point. In fact, it misses this point just by a little and it is therefore possible to establish the displayed continuous variation within a range of 0.0002 Å from the ridge.

If one substitutes the expansion of the diabatic states (as given by Fig. 9) in the transformation to the adiabatic states [as given by Eq. (10) and Fig. 10], then one obtains the expansions of the adiabatic states in terms of the four configurations. The resulting coefficients are displayed in Fig. 11 and behave in agreement with Table I. These coefficients were, of course, the starting point of our calculations from which the data of Figs. 9 and 10 were deduced as outlined in Sec. II D 2.

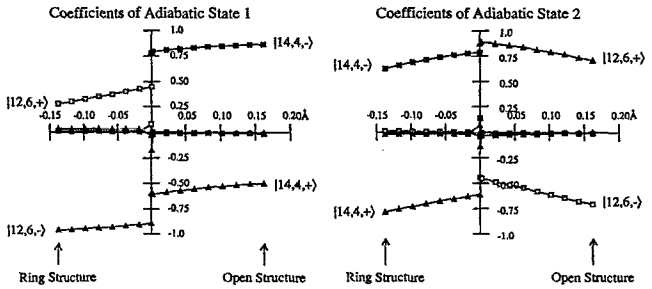

FIG. 11. Variation of the coefficients of the adiabatic states along the path between the ground state minima.

C. Configurational analysis of ΔH and H_{12} along the line connecting the two minima

1. Analysis of ΔH

The upper panel of Fig. 12 contains plots of *the energies of the four configurations as dotted lines.* Round symbols denote the two configurations that would appear in a SCF calculation and diamond symbols indicate the two configurations that are the dominant correlation-type configurations.

The solid symbols correspond to the $|12,6\rangle$-type configurations. At the ring structure, $|12,6,+\rangle$ is much more stable than $|12,6,-\rangle$. This is because here σ_+ is a bonding MO, whereas σ_- is antibonding. At the open structure, the configurations have, however, almost equal energies, since at that distance of the end atoms from each other, σ_+ and σ_- are both nonbonding MOs.

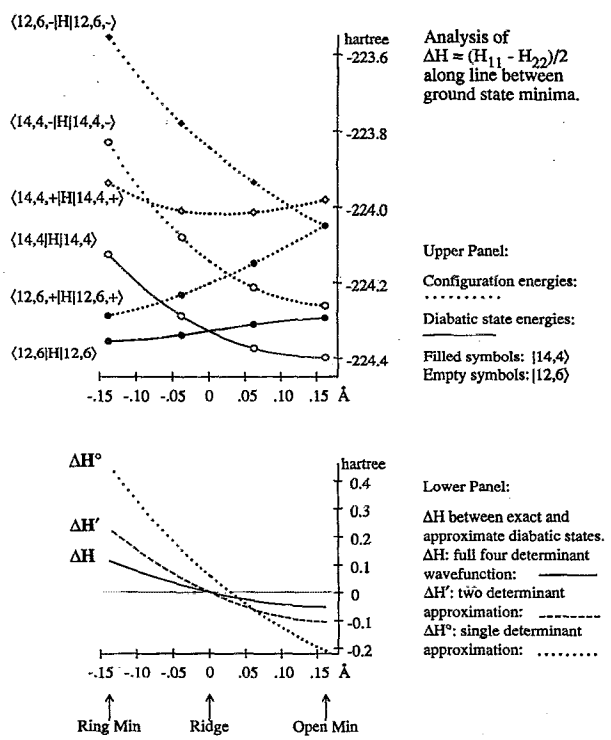

FIG. 12. Decomposition of ΔH in terms of configurational contributions.

The open symbols correspond to the $|14,4\rangle$-type configurations. At the open structure, $|14,4,-\rangle$ is more stable than $|14,4,+\rangle$ because here π_- is a nonbonding MO, whereas π_+ is an antibonding MO. However, at the ring structure, the energies of the two configurations are quite close to each other, since for exact D_{3h} symmetry, the orbitals π_+ and π_- would be degenerate.

It is also apparent that, for the ring structure, the configuration $|12,6,+\rangle$ is much lower in energy than both $|14,4\rangle$ configurations, whereas for the open structure, the configuration $|14,4,-\rangle$ is much lower in energy than both $|12,6\rangle$ configurations. *Thus, the bonding/nonbonding/antibonding effects of the four molecular orbitals for the various geometries straightforwardly explain the crossover of the energies of the diabatic states which are displayed by the two solid lines and which account for the sign change of ΔH.*

The lower panel of Fig. 12 exhibits the values obtained for $(H_{11}-H_{22})/2$ by (i) using the full four-configuration expression (labeled ΔH); (ii) using only the two dominant configurations in each diabatic wave function (labeled $\Delta H'$); (iii) using only the SCF determinants $|12,6,+\rangle$ and $|12,6,-\rangle$ in the calculation (labeled ΔH^0). It shows that the dominant configurations determine the overall character of the ΔH curve.

2. Analysis of H_{12}

We saw that the sign change in ΔH can be easily traced to changes in orbital stabilities caused by changing bonding/nonbonding/antibonding interactions. Such changes of $(H_{11}-H_{22})$ with changing molecular geometries are extremely common. Sign changes in H_{12}, on the other hand, are more difficult to understand. Here, they are crucial. Wherever H_{12} is nonzero, an *avoided* crossing occurs when ΔH changes sign. *The occurrence of a true crossing hinges on H_{12} changing sign in addition to ΔH doing so.*

For an explanation of the behavior of H_{12}, it is sufficient to use the expansion of the diabatic states in terms of their respective two dominant configurations, viz.,

$$|12,6\rangle = a_+|12,6,+\rangle + a_-|12,6,-\rangle,$$
$$|14,4\rangle = b_+|14,4,+\rangle + b_-|14,4,-\rangle. \quad (11)$$

The values for the coefficients in these equations are obtained from those on the left-hand graphs of Fig. 9 by renormalization. It is apparent that a_+ and b_- are positive, whereas a_- and b_+ are negative. With these (approximate) expansions, the off-diagonal Hamiltonian matrix element becomes a sum of four terms

$$\begin{aligned} H_{12} &\approx \langle 12,6|H|14,4\rangle \\ &\approx a_+b_+\langle 12,6,+|H|14,4,+\rangle \\ &\quad + a_+b_-\langle 12,6,+|H|14,4,-\rangle \\ &\quad + a_-b_+\langle 12,6,-|H|14,4,+\rangle \\ &\quad + a_-b_-\langle 12,6,-|H|14,4,-\rangle. \end{aligned} \quad (12)$$

The solid lines in the top panel of Fig. 13 display the quantitative values of the four terms in Eq. (12) along the line connecting the two minima. The values plotted are the

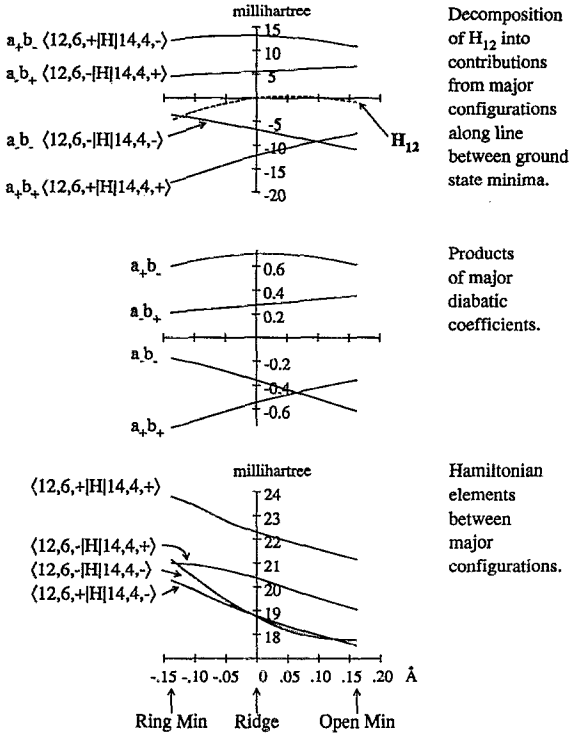

FIG. 13. Decomposition of H_{12} in terms of configurational contributions.

matrix elements multiplied by the coefficients. The sum of the four contributions is the dotted curve which is practically identical with the exact H_{12} curve in the lower right panel of Fig. 7. It is apparent that the reason for the sign change in the H_{12} curve is the fact that *the negative contributions change significantly in magnitude along the path.*

The lower two panels provide the decomposition of the contributions shown in the top panel in terms of the orbital coefficient products and the matrix elements between the configurations. The former are displayed in the middle panel, the latter are exhibited in the bottom panel. An examination of these two panels reveals that the variations of the contributions on the top panel are due to the variation of the coefficient products and not to those of the matrix elements between the configurations. Note that the negative contributions on the top and middle panels change by factors of 2–3, whereas the matrix elements in the bottom panel vary only by about 10%. Moreover, the matrix elements are all positive because all four configurations differ from each other in doubly occupied orbitals so that all matrix elements are exchange integrals.

The sign change of H_{12} is thus related to the changes in the negative coefficient products in the middle panel. The latter are, however, a direct consequence of the *changes in the relative weights of the dominant configurations within each diabatic state* which we discussed in detail in Sec. III B 1. There exist many examples of two diabatic states exchanging dominance in two adiabatic states, where each diabatic state contains only *one* dominant configuration and where these *two dominant configurations* differ by a doubly occupied orbital. In these common cases, the matrix element H_{12} is approximately the exchange integral $\langle uv|r_{12}^{-1}|uv\rangle$ between those orbitals in which the two dominant configurations differ. Since such integrals are always positive, *they cannot change signs.* Consequently, the reason for the possibility of a conical intersection in the present case is *the presence of more than one dominant configuration in each diabatic state* and the fact that, on the path from one minimum basin to another, *not only do the diabatic states exchange dominance in the adiabatic states but, moreover, that there occurs an internal exchange of dominance between configurations within each diabatic state.* The reasons for these changes in the weights of the configurations were explained in Sec. III B.

IV. CONCLUSIONS

The two lowest $^1A_1$ states of ozone (the lower one being the ground state) have been decomposed in terms of two diabatic states by application of the quantum chemical method formulated in the subsequent paper.[3] The examination of the configurational expansions of these *diabatic* states has led to the identification of those features of the electronic structure which are responsible for the occurrence of the conical intersection between these two *adiabatic* closed-shell states of like symmetry.

It is concluded that, in cases where the dominant configurations of the diabatic states contain only doubly occupied orbitals, as is common for ground states, an intersection can occur only if each diabatic state itself contains more than one dominant configuration and if, in addition, the weights of these configurations within the diabatic states change significantly in the region of the coordinate space where the intersection occurs. In other words, intersections between closed-shell singlets of like symmetry *cannot* be expected if the *diabatic* states contain only *dynamic* correlations. They *can* occur if *the diabatic states* embody *nondynamic* correlations and if, moreover, strong *shifts* occur in the latter. Such shifts can result from changing bonding interactions.

ACKNOWLEDGMENTS

The authors gratefully acknowledge the preliminary work by A. A. Nanayakkara and K. Ruedenberg mentioned in Ref. 5. The present work was supported by the Division of Chemical Sciences, Office of Basic Energy Sciences, U.S. Department of Energy. The Ames Laboratory is operated for the U.S. Department of Energy by Iowa State University under Contract No. W-7405-Eng-82.

[1] S. Xantheas, G. J. Atchity, S. T. Elbert, and K. Ruedenberg, J. Chem. Phys. **94**, 8054 (1991).

[2] (a) G. Herzberg and H. C. Longuet-Higgins, Discuss. Faraday Soc. **35**, 77 (1963); see also M. V. Berry, Proc. R. Soc. London Ser. A **392**, 45 (1984); C. A. Mead, J. Chem. Phys. **70**, 2276 (1979); C. A. Mead and D. G. Truhlar, *ibid.* **70**, 2284 (1979); (b) G. J. Atchity, S. S. Xantheas, and K. Ruedenberg, *ibid.* **95**, 1862 (1991).

[3] K. Ruedenberg and G. Atchity, J. Chem. Phys. **99**, 3799 (1993).

[4] (a) K. R. Sundberg and K. Ruedenberg, *Quantum Science*, edited by J. L. Calais, O. Goscinski, J. Linderberg, and Y. Ohrn (Plenum, New York, 1976), p. 505ff; M. Gilbert-Dombek, Ph.D. thesis, Iowa State University, 1977; K. Ruedenberg, *Proceedings of the August 1978 NRCC Workshop on Post-Hartree–Fock Quantum Chemistry and Configuration Interaction* (Lawrence Berkeley Laboratory, University of

California, 1979), p. 46; L. M. Cheung, K. R. Sundberg, and K. Ruedenberg, Int. J. Quantum Chem. **16**, 1103 (1979); K. Ruedenberg, M. W. Schmidt, M. M. Gilbert, and S. T. Elbert, Chem. Phys. **71**, 41 (1982); **71**, 51 (1982); **71**, 65 (1982); (b) P. E. H. Siegbahn, A. Heiberg, B. O. Roos, and B. Levy, Phys. Scr. **21**, 323 (1980); B. O. Roos, P. R. Taylor, and P. E. M. Siegbahn, Chem. Phys. **48**, 157 (1980).

[5]Such calculations in the entire FORS space were made near the intersection by A. Nanayakkara and K. Ruedenberg. They gave results for ΔH and H_{12} in very close agreement with those displayed in Fig. 8 below.

[6]T. H. Dunning and P. J. Hay, in *Methods of Electronic Structure Theory*, edited by H. F. Schaefer (Plenum, New York, 1977), Vol. 3, p. 1.

[7]H.-J. Werner and P. J. Knowles, J. Chem. Phys. **82**, 5053 (1985); Chem. Phys. Lett. **115**, 259 (1985).